Biosensors and Bioelectronics 71 (2015) 261–268

Contents lists available at ScienceDirect

Biosensors and Bioelectronics

journal homepage: www.elsevier.com/locate/bios

A third-order mode high frequency biosensor with atomic resolution

Hua-Lin Cai [a,b], Yi Yang [a,b], Xiao Chen [a,b], Mohammad Ali Mohammad [a,b], Tian-Xiang Ye [a,b], Cang-Ran Guo [c], Li-Ting Yi [c], Chang-Jian Zhou [a,b], Jing Liu [c], Tian-Ling Ren [a,b,*]

[a] Institute of Microelectronics, Tsinghua University, Beijing 100084, China
[b] Tsinghua National Laboratory for Information and Science Technology (TNList), Tsinghua University, Beijing 100084, China
[c] Department of Biomedical Engineering, Tsinghua University, Beijing 100084, China

ARTICLE INFO

Article history:
Received 29 December 2014
Received in revised form
19 March 2015
Accepted 14 April 2015
Available online 15 April 2015

Keywords:
SAW biosensor
High frequency
DNA
Cancer cell
Atomic resolution
Label free

ABSTRACT

An atomic resolution ultra-high sensitivity surface acoustic wave (SAW) biosensor for DNA sequences and cells detection is proposed. Interdigitated transducers (IDTs) fabricated on $LiNbO_3$ substrate achieve a high quality factor (*Q*) of over 4000 at a frequency of 6.4 GHz (third-order harmonic mode) using an optimized design and process. The biosensor shows excellent linear responses to target DNA in the range from 1 μg/ml to 1 ng/ml with a high sensitivity of 6.7×10^{-16} g/cm^2/Hz, hence the difference of a single hybridized DNA base can also be distinguished. With such a high mass resolution, the biosensor is capable of quantitative detection of living cancer cells. The frequency responses of single mouse mammary adenocarcinoma (EMT6) cell and mouse fibroblast (3T3) cell are studied. The interferences in the experiments show insignificant influence on the frequency shift, which verifies the high selectivity of the biosensor. The biosensor is also able to repeat the sensing ability after rough cleaning, therefore cost reduction is achieved from the recycling process in practical applications. The detection limit is defined from the noise analysis of the device, atomic resolution is realized according to the calculation, thereby initiating a potential tool for high-precision medical diagnoses and phenomena observation at the atomic-level.

1. Introduction

High sensitivity, high selectivity and rapid response label-free biosensors suitable for field use or point-of-care applications are extensively used in disease diagnoses and other fields (Alivisatos, 2004; Giljohann, et al., 2009; Rosi et al., 2005). It is imperative to develop techniques capable of detecting ultra-low concentration samples or even single molecules and atoms (Jensen et al., 2008; Naik et al., 2009; Yang et al., 2006). This will enable the reliable detection of certain biochemical reaction mechanisms, such as DNA hybridization, intracellular mutations, etc. Numerous biosensors have been made by utilizing novel materials (Heller et al., 2009; Lu et al., 2011; Mannoor et al., 2012; Peng et al., 2009), structures (Dong et al., 2010; Feng et al., 2008; Li et al., 2007; Venkatesan et al., 2011) and methods (Aebersold et al. 2003; Anker et al., 2008; Lee et al., 2008; Sun et al., 2013) or combinations of them to break previous performance limitations. However, these works contain various drawbacks for real-world applications. For example, some of these devices contain mechanical parts which lack durability, or which cannot sustain repeated immersion in liquids for reliable detection, etc. Other approaches either need complicated device fabrication process or require complex sample purification and subsequent amplification steps, which make the detection very costly and time-consuming. SAW devices are an exciting alternative for biomedical applications. These devices do not contain any mechanical parts and are therefore a robust sensing platform. SAW devices have previously been used with a resonant frequency of over 1 GHz for highly sensitive detection (Krishnamoorthy, et al., 2008; Kim et al., 2013). In order to obtain an even higher sensitivity, it is desirable to increase the resonant frequency (Petrie et al., 2011). Super high frequency (SHF) resonators are able to provide unprecedented sensitivity for mass sensing and real-time measurement. Additionally, these devices are also able to ease the requirements of large complex equipment and therefore enable a greater portability and cost effectiveness. Various complex nano devices have been fabricated which have demonstrated great potential for chemical and biomedical sensing applications (Chen et al., 2011; Dow et al., 2012; Palankar et al., 2013; Shi et al., 2010). SAW devices have a relatively short and straightforward fabrication process and are a simple sensing platform with a high frequency and *Q*. Nevertheless, it is still challenging to fabricate high-performance SAW devices due to a number of factors. The use of non-conducting substrates

* Corresponding author at: Institute of Microelectronics, Tsinghua University, Beijing 100084, China.
E-mail address: RenTL@tsinghua.edu.cn (T.-L. Ren).

http://dx.doi.org/10.1016/j.bios.2015.04.043
0956-5663/

introduces charging during electron beam lithography (EBL) which needs to be corrected using conductive top-coating (Muhammad et al., 2011; Peters et al., 2013). The dense IDTs are adversely affected due to proximity effect during EBL which needs to be corrected by software or avoided by careful process parameter selection.

In this paper, a SAW biosensor with an atomic resolution has been developed. IDTs of 500 nm width and a 2 μm period provide a super high resonant frequency of 6.4 GHz (third order mode) and a *Q* of over 4000. For the purpose of biosensing, using such a high frequency is unprecedented. When the samples are immobilized on the delay area of the biosensor, the resonant frequency of the device is decreased in response to the adsorbed mass. By measuring the frequency shifts, the immobilized mass is obtained. In this way, highly sensitive and selective measurements for ultralight mass can be performed with very simply processed samples. By employing these devices, a single DNA base difference can be detected. Meanwhile, linear frequency response for a varying number of EMT6 cells and 3T3 cells in a wide number concentration range is achieved. The capacity of single cell detection is expected to realize accurate diagnoses of individual cellular mutation, lesion, dynamic change, etc. The biosensor is an ideal solution to sequence entire genomes, detecting markers of disease at a very low concentration and understanding the molecular basis of disease. For instance, by distinguishing the mass differences among the four kinds of DNA bases, the base type in a DNA chain is easily known. The detection accuracy is guaranteed and the cost reduction is realized. It is difficult to diagnose the existence of antigen, bacteria or virus at an early stage because of the low concentration in organisms. This, however, is detrimental to the health of the organisms and causes irreparable harm. The biosensor has the ability to detect very atomic-level mass changes caused by specific binding to detect the lesion. Moreover, the blood glucose, protein or other biological and chemical substances and their concentration are also detectable on account of the reaction or consumption of them on the biosensor. These applications demonstrate that the SAW biosensor offers exciting possibilities for ultra-high-precision mass discrimination.

2. Material and methods

2.1. Device fabrication

The resist was spin-coated on a $LiNbO_3$ substrate and a thin layer of 5 nm Cr was sputtered on top to improve the substrate conductivity. EBL (JEOL 6300FS, 100 keV) was used to pattern the SAW IDTs and delay area. This is followed by removing the thin Cr layer, sputtering 50 nm gold and performing lift-off. (See supplementary materials)

2.2. FEM simulation and principle analysis

The design of the SAW biosensor is optimized by Finite Element Method (FEM) simulation. Firstly, the three-dimension model is created with the practical device parameters. Frequency sweep signal is added on the device to show the spectrum. Secondly, the parameters such as the thickness of the metal, the number and the space of IDTs are gradually changed to optimize the performance of the device. Representative simulated results are shown in Fig. 1a. Left panel shows the surface wave transmission map of the device, it is the resonance of IDTs on the substrate, and the red part shows where the resonance is the strongest. The right panel shows the harmonic analysis results. In the right panel, the displacement amplitude (normalized to the maximum value) is a function of the applied AC signal frequency and the resonant modes can be clearly observed. The third-order harmonic, which still has a large resonant amplitude and an excellent *Q* of over 4000, is applied for detection and the measured resonant frequency is about 6.4 GHz. The *Q* is calculated from the measured reflection coefficient S_{11} using the equation $Q=f/BW$, where f is resonant frequency, and BW is 3 dB bandwidth.

The surface acoustic waves generated by the IDTs propagate along the surface of the substrate at a certain depth. Upon reaching the delay area, these waves will partially reflect. When target substances are immobilized and hybridized on the delay area, a thin superimposed molecular film is formed, which effectively alters the film thickness and density. This causes the velocity of the reflected signal to change, which in turn shifts the resonance frequency (Fig. 1b) according to the equation $f=v/\lambda$, where f is resonant frequency, v is the velocity of surface wave, and λ is wavelength of surface wave. Furthermore, due to the addition of the molecular film on the delay area, there is an increased dissipation of energy causing a reduction of the biosensor *Q*-factor.

Fig. 1c shows the Scanning electron microscope (SEM) of the fabricated SAW IDTs, bonding pad and partially amplified views of the SAW device. The IDT array of the SAW devices are 60 μm wide and 1000 μm long. These IDT arrays attach to two electrodes (60 μm by 200 μm), one of which is connected to the signal port and the other to ground. The size of the delay area used for sample immobilization is 1 mm × 1 mm. Each IDT has a finger width and spacing of 500 nm, which indicates that the wave length λ of the device is 2 μm and the calculated resonant fundamental frequency is about 2 GHz. Fig. 1d shows the probe DNA's immobilization on the gold delay area surface followed by hybridization of the target DNA with the probe DNA. Both attachment steps yield mass and resonant frequency changes.

2.3. Biological treatment

The DNA detection is based on the probe–target DNA binding mechanism (Fig. 1d) and the immobilization of DNA on delay area is shown in Fig. 2a and b. When DNA is immobilized and hybridized on the delay area, the surface has an obvious change that indicates the existence of DNA molecules.

The probe DNA is first immobilized on the gold surface of the delay area, which causes a frequency shift. This is due to the reduction of velocity of the surface acoustic wave through the immobilized molecular film. Then the target DNA is hybridized with the probe DNA under specific conditions to cause an additional frequency shift. By measuring the frequency shifts, the immobilized mass that indicates the DNA solution concentration can be calculated.

A method that improves the immobilization of DNA molecule with gold surface was applied for reliable analysis of the sensing effect (Lucarelli et al., 2008; Peterson et al., 2001; Petrovykh et al., 2003; Smith et al., 2001). To exclude the defects in the DNA hybridization processes, several contrast experiments that exclude the influence of other substances were also conducted to guarantee the validity of the results. The basic DNA immobilization and hybridization flow is described below: (1) The thiol-modified probe DNA (pDNA) solution for immobilization is prepared by mixing with the Phosphate Buffered Saline (PBS, 0.01 M PH=7.4). (2) The gold delay area is rinsed with a Piranha solution (70% H_2SO_4 and 30% H_2O_2) to clean the surface and strengthen the molecular adhesion. (3) The pDNA mixed with a 0.1 M KNO_3 solution is injected on the delay area, and then stored in a 4 °C chamber with proper humidity for 24 h to allow the pDNA to fully immobilize. (4) The delay area is washed with Milli-Q water and then dried with N_2 followed by covering a 1ng/ml bovine serum albumin (BSA) to block the uncovered gold surface. (5) The target

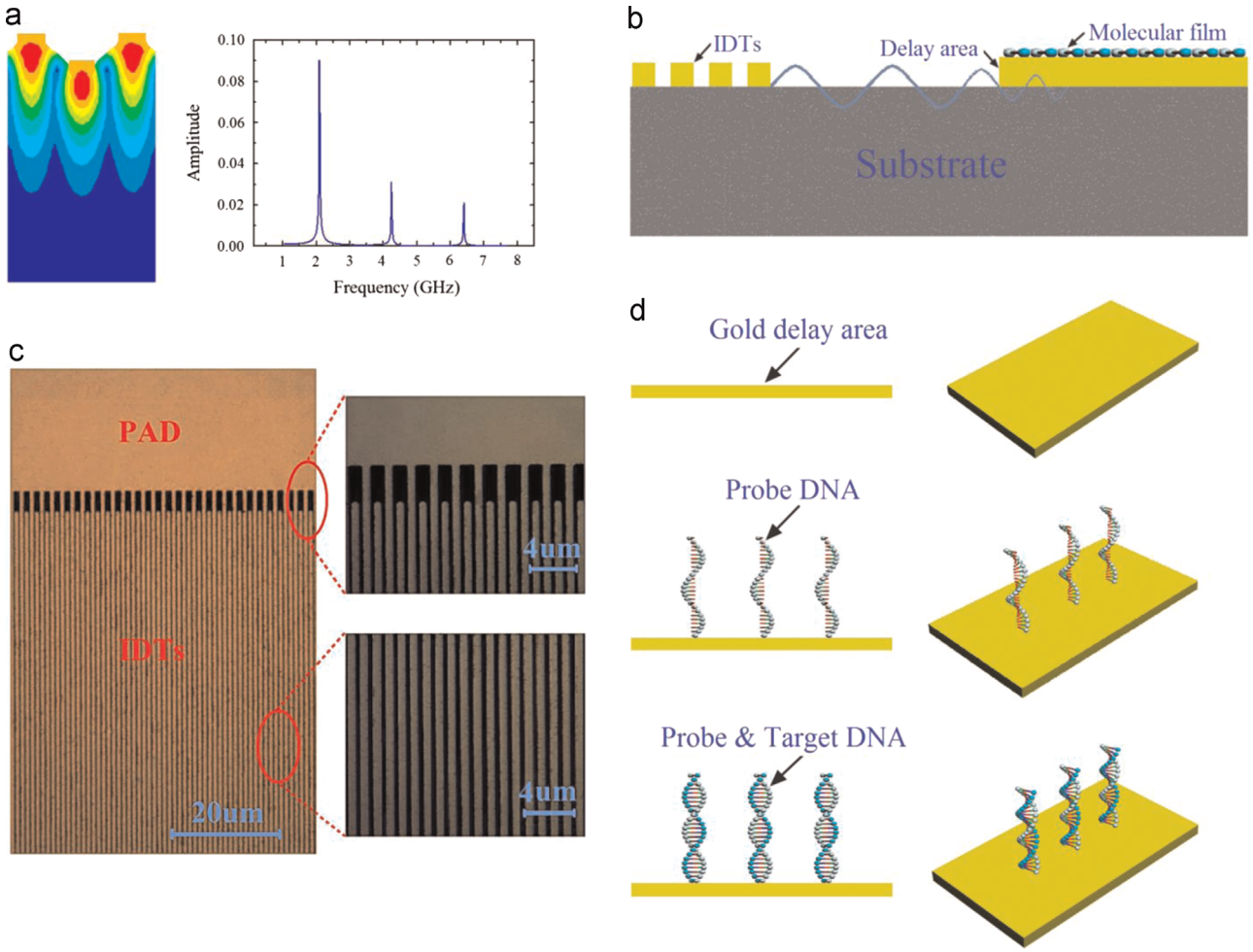

Fig. 1. (a) FEM modeling of the high frequency SAW device. (b) The effect of molecules' immobilization on delay area and the sensing mechanism illustration of the biosensor. (c) Scanning electron microscope (SEM) of the fabricated SAW IDTs, bonding pad and partially amplified views of the SAW device. (d) Process showing probe DNA immobilization on the gold delay area surface followed by hybridization of the target DNA with the probe DNA.

DNA (tDNA) is injected on the delay area and then stored in a 4 °C chamber for 4 h to make it completely hybridize with the pDNA. (6) The delay area is washed with PBS to remove the unhybridized tDNA followed by N_2 drying.

The detection of cells is based on measuring the frequency shift caused by the adsorbed mass of cells on the delay area. Various cell masses will cause various frequency shifts, which can be used for quantitative analysis of the immobilized cells. After Piranha cleaning of the surface of the gold delay area, the solutions that contain the EMT6 cells and the 3T3 cells are respectively applied to the delay area followed by N_2 drying. The resonant characteristics of the biosensor are continuously observed until the frequency and amplitude of the reflection coefficient (S_{11}) is stable. The S_{11} is recorded at this point indicating reliable immobilization of cells and the inexistence of surface moisture. Because the time duration for the measurement is short, the cell proliferation that will cause extra mass addition is negligible. Fig. 2c and d shows the immobilization of the EMT6 cells and the 3T3 cells on delay area.

2.4. Measurement conditions

All measurements are performed under 25 °C in a clean room to avoid fluctuations and interferences. The SAW device is electrically connected to a printed circuit board (PCB) through bonding wires. The electrical performances of the SAW devices are characterized by an Agilent 8722ES vector network analyzer (VNA). The IDTs and the bonding wires are covered to protect them from harsh biochemical operations.

3. Results and discussion

3.1. DNA detection

The frequency shifts with the same pDNA concentration (3 μg/ml, 3′-SH-AAAAAAAAAACCCCCACTAAAAGGTCCTAAAAACCTAAAAACCT-5′) and gradually altered tDNA (5′-TCCAGGATTTTTGGA-3′) concentrations of 1 ng/ml (Fig. 3a), 10 ng/ml (Fig. 3b), 100 ng/ml (Fig. 3c) and 1 μg/ml (Fig. 3d) show a wide detection range and a good linearity (Fig. 3e). In Fig. 3, the black line is the original resonant frequency of the biosensor, the red line is the resonant frequency with the immobilization of probe DNA, and the blue line is the resonant frequency with the hybridization of target DNA.

The contrast hybridization experiments of short chain tDNA with 4 bases and 3 bases (5′-TTTT-3′,5′-TTT-3′) cause frequency shifts that are approximately in proportion to the length of the DNA chain. The molarity of both DNA bases is the same as the sample shown in Fig. 3d. Fig. 4a and b shows that the difference of a single DNA base can be distinguished. In order to verify the complementary probe–target DNA binding mechanism of the SAW biosensor, the frequency responses for mismatched tDNA with the same pDNA concentration are also studied. The tDNA with one

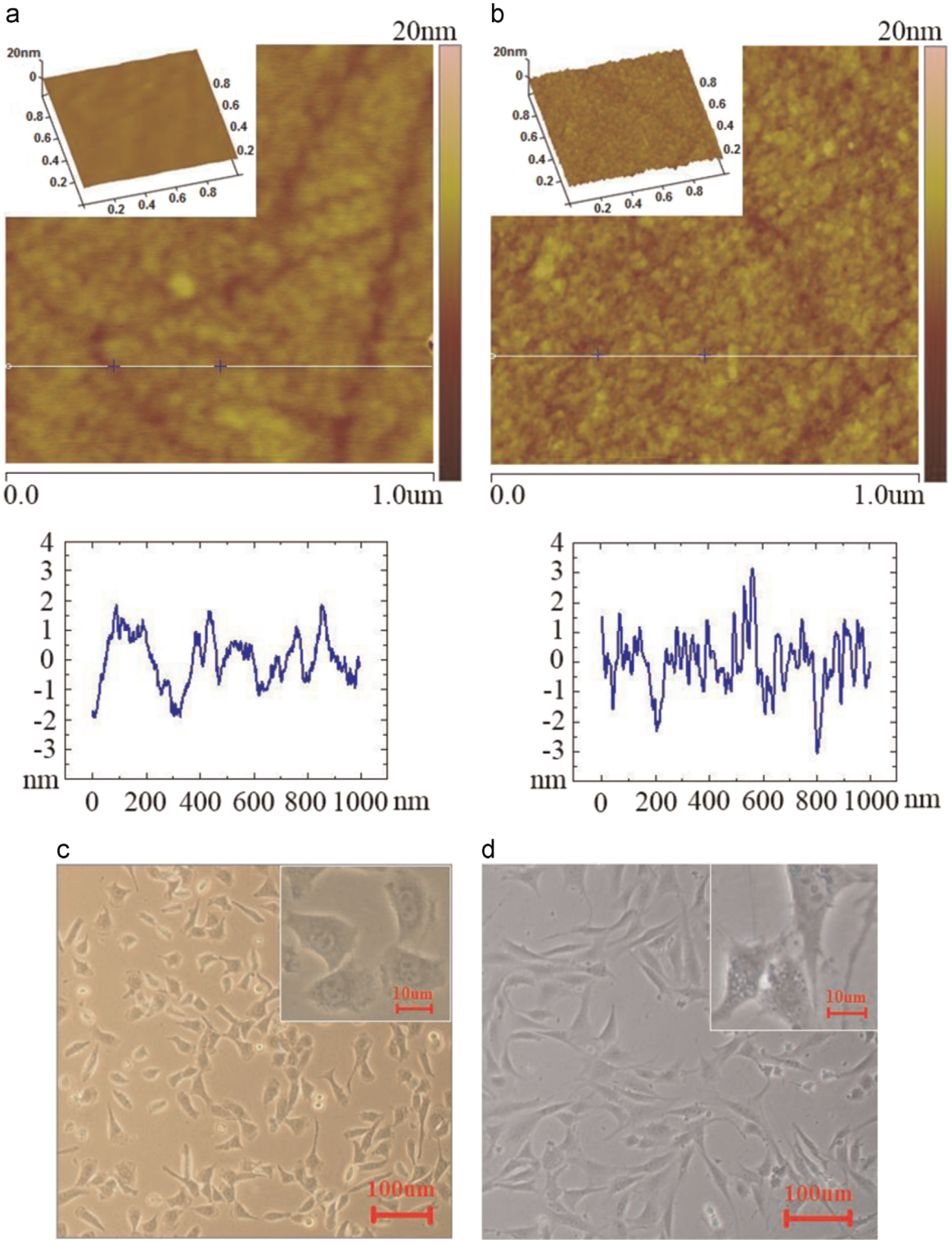

Fig. 2. (a) AFM scans comparing the biosensor delay area without DNA. (b) AFM scans comparing the biosensor delay area with DNA. (c) The immobilizations of EMT6 cells on the device delay area. (d) The immobilizations of 3T3 cells on the device delay area.

base mismatch (5′-TCGAGGATTTTTGGA-3′) and two base mismatches (5′-TCGAGGATTATTGGA-3′) have lower frequency shifts than the complementary tDNA (shown in Fig. 4c and d). The influences on the frequency shifts due to interfering substances such as BSA and PBS are also investigated. Fig. 4e and f presents the contributions to the frequency shifts due to them. Moreover, detecting the comparatively small shift caused by BSA and PBS indicates the high selectivity of the SAW biosensor. Several samples were measured and all of them achieved the same trend, which attests to the uniformity of the fabricated devices.

All the frequency shift responses of target substances based on the same pDNA concentration are shown in Fig. 5. The numbers of target substances are labeled according to the corresponding figure numbers in this paper (e.g. the sample 7d represents the target substance response shown in Fig. 3d). It is a clear comparison of the detection results. The first column shows the frequency shift

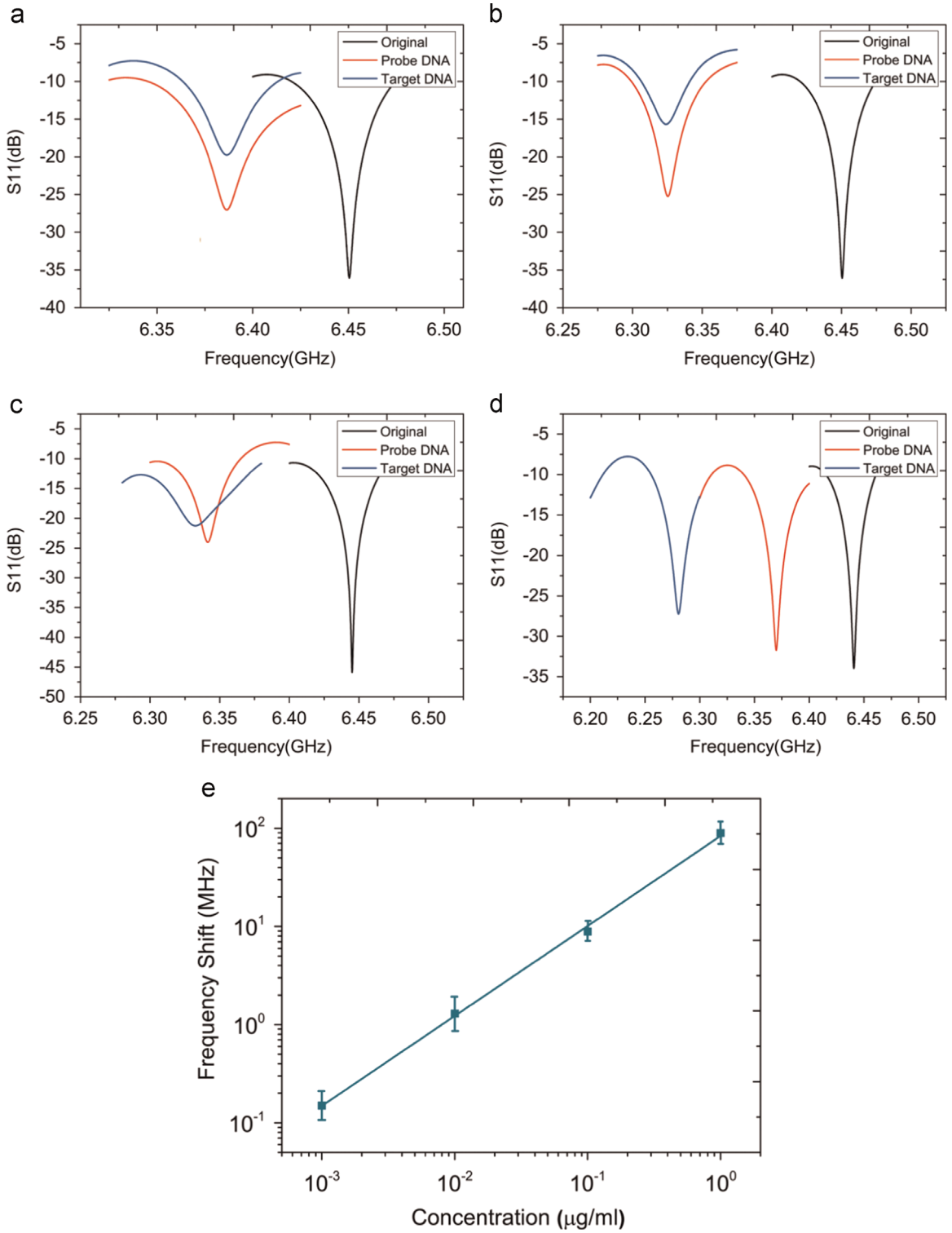

Fig. 3. Frequency shifts for target DNA concentrations of (a) 1 ng/ml, (b) 10 ng/ml, (c) 100 ng/ml, and (d) 1 μg/ml, with a probe DNA concentration of 3 μg/ml. (e) Correlation analyses between target DNA concentrations and frequency shifts (For interpretation of the references to color in this figure the reader is referred to the web version of this article.).

with immobilization of sample 7d. This sample has a concentration of 1 μg/ml with 15 bases. Sample 10a has the same concentration, but one base is mismatched, so the frequency shift is lower. The frequency shift of sample 10b is even lower than the frequency shift of sample 10a because there are two mismatched bases. Sample 9a has a concentration of 1 μg/ml, but the base number is four, so the frequency shift is decreased according to the overall mass reduction. The sample 9b causes even lower frequency shift than sample 9a because the base number of it is three. Samples 7c, 7b, and 7a all cause proportional frequency shifts based on their concentration. Samples 11a and 11b show little contribution of interference such as from BSA and PBS to frequency shift.

After the ultrasonic cleaning of the delay area, the

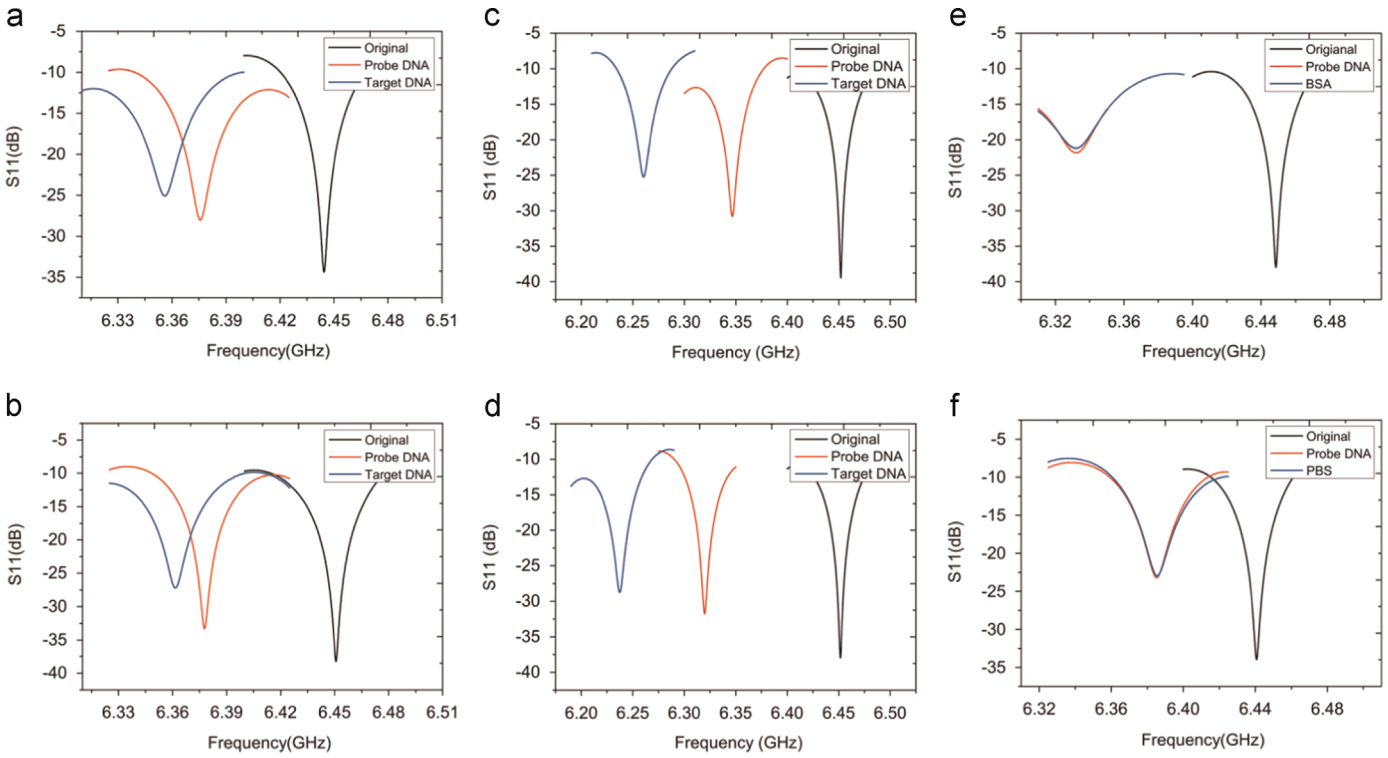

Fig. 4. The frequency shifts with (a) 4 bases and (b) 3 bases that have the same target DNA molarity with sample 7d. The frequency shifts with (c) 1 DNA base mismatch, and (d) 2 DNA base mismatches that have the same target DNA molarity with sample 7d.The frequency responses of (e) BSA and (f) PBS.

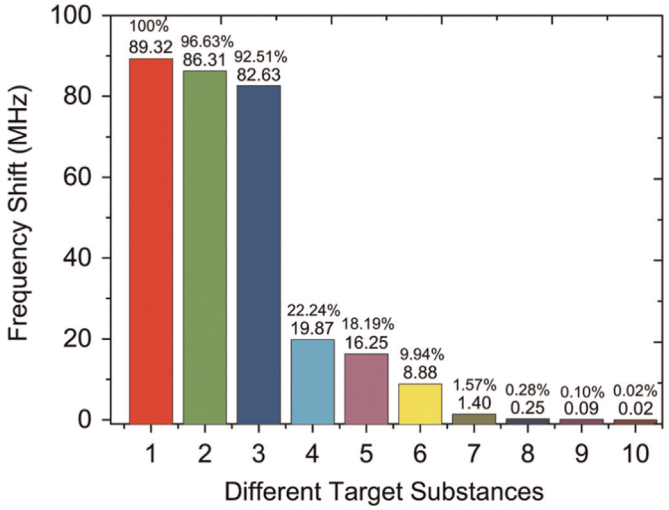

Fig. 5. The frequency shift comparisons with different target substances. (1) Sample 7d: 1 μg/ml with 15 bases (2) Sample 10a: 1 μg/ml with 15 bases, one base mismatch with Sample 7d (3) Sample 10b: 1 μg/ml with 15 bases, two base mismatch with Sample 7d (4) Sample 9a: 1 μg/ml with 4 bases (5) Sample 9b: 1 μg/ml with 3 bases (6) Sample 7c: 100 ng/ml with 15 bases (7) Sample 7b: 10 ng/ml with 15 bases (8) Sample 7a: 1 ng/ml with 15 bases (9) Sample 11a:BSA (10) Sample 11b: PBS.

immobilization process was repeated with DNA sample 7d and the frequency response was obtained (See Fig. S2 in Supplementary materials). The device is able to conduct multiple sets of detections with unaltered properties. This repeatability and the ability to recycle is of great importance to reduce the cost, which is one of the main considerations in future commercial applications.

3.2. Detection of cells

EMT6 cells and 3T3 cells are different cells that characterize different mass and size. Detecting these differences requires a highly sensitive sensor. Six sets of EMT6 and 3T3 cell solutions with a number concentration of 10^7/ml, 10^6/ml, 10^5/ml, 10^4/ml, 10^3/ml and 10^2/ml are used to detect the responses of the biosensor to them. A 10 μL volume of cell solution is dropped on the delay area for each immobilization. Fig. 6a and b shows the frequency responses for EMT6 cells and 3T3 cells. A greater cell immobilization on the delay area will cause a larger frequency shift. Fig. 6c shows the frequency shifts between EMT6 cells and 3T3 cells for a varying number of cells. The two lines in Fig. 6c are obtained by linear fitting analysis of the achieved frequency shift points. It can be easily observed for both sets of cells through the trend that the ability of single cell detection is realized, which is shown in Fig. 6c. Due to the high sensitivity, it is able to perform accurate analysis of the intracellular mutation or lesion that will cause extra mass and size changes (de la Rica et al., 2009).

3.3. Noise analysis

The Sauerbrey equation (Campanella et al., 2006; Ferreira et al., 2009) (Eq. (1)) relates the addition of mass to the change in resonant frequency. This equation can be used to explain the linear relationship (see Fig. 6c) between the immobilized mass and the resonant frequency shift of the SAW devices. The Sauerbrey equation can be written as,

$$\frac{\Delta f}{f_0} \approx -\frac{\rho_m t_m}{\rho_0 t_0} = -\frac{\Delta m}{m_0} \quad (1)$$

where m_o is the equivalent mass of the resonant part of the device, ρ_m and t_m are the density and thickness of the immobilized DNA, and the mass change Δm due to the DNA causes a frequency shift Δf for a device that has a resonant frequency f_0. Based on the measured results, the sensitivity is calculated according to Eq. (2).

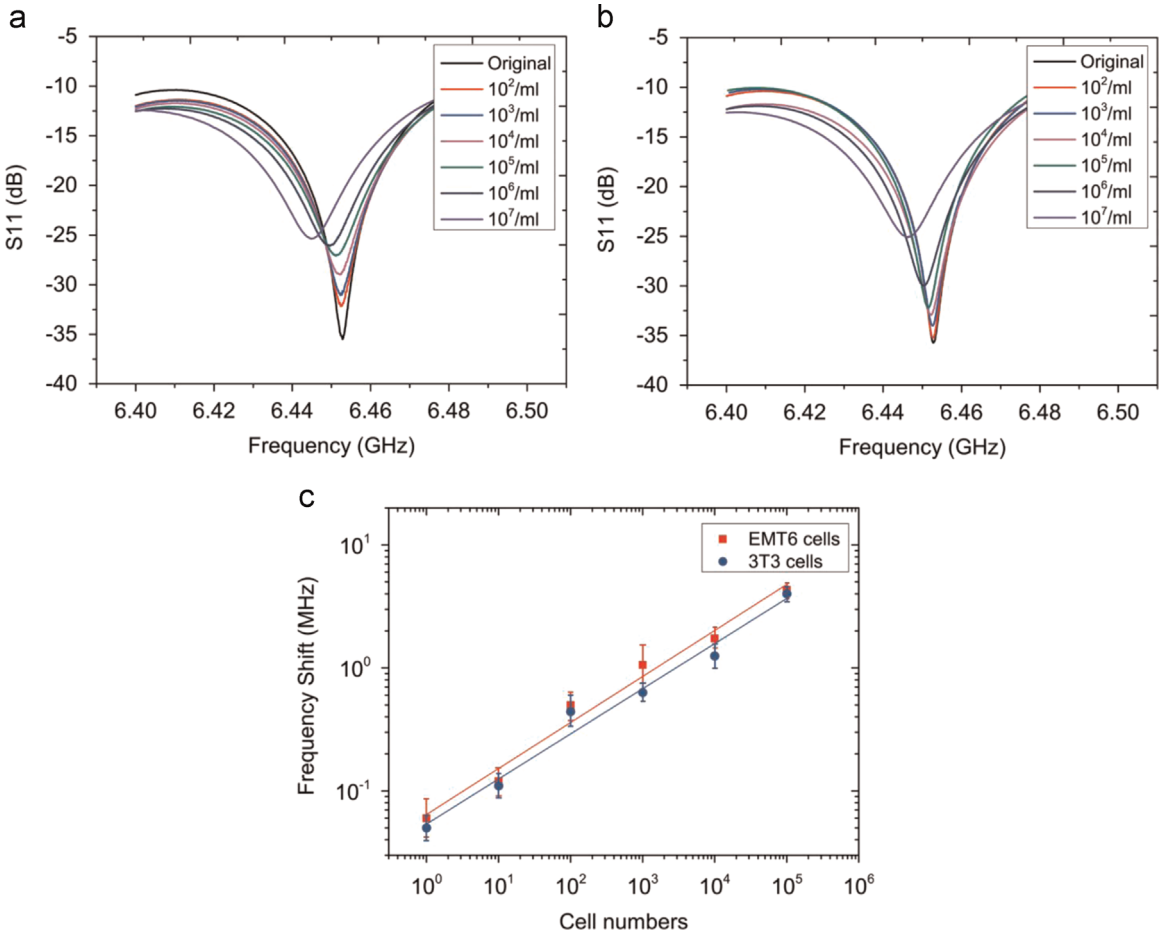

Fig. 6. The frequency shift responses for gradually changed number of (a) EMT6 cells and (b) 3T3 cells. (c) The frequency shifts due to immobilization of EMT6 cells (square) and 3T3 cells (circles).

$$S = \frac{\Delta m'}{\Delta f} = \frac{C \cdot V}{\Delta f \cdot A} \tag{2}$$

where the sensitivity S is defined as the frequency shift Δf that is caused by the mass change of a unit area $\Delta m'$. C is the concentration of the DNA solution, A is the area of the delay area and V is the volume of the added DNA solution. According to Eq. (1), we have the derivation shown in Eq. (3).

$$\frac{m_0}{f_0} = -\frac{\Delta m}{\Delta f} = -\frac{A \cdot \Delta m'}{\Delta f} \tag{3}$$

The frequency of unloaded device will vary under constant conditions. This variation or "noise" can be expressed as a fictional mass which can be used to calculate mass noise floor of the biosensor, as is shown in Eq. (4).

$$\Delta m_2' = \frac{\Delta m_1'}{\Delta f_1} \cdot \Delta f_2 = S \cdot \Delta f_2 \tag{4}$$

where the $\Delta m'_1$ is the mass change per unit area, Δf_1 is the frequency shift due to the mass change, $\Delta m'_2$ is the equivalent mass noise per unit area, and Δf_2 is the maximum frequency variation noise. The resonant frequency varies with time under constant conditions as shown in Fig. S3a in supplementary materials. The maximum frequency variation is about 260 kHz and the corresponding $\Delta m'_2$ is 1.74×10^{-10} g/cm^2 for the achieved sensitivity.

From the data in Fig. S3a, we calculate 6.45175 GHz as the time-average center frequency. The frequency variation data is gathered under large discrete time intervals, so it is necessary to calculate the probability for the obtained result. Therefore, 400 resonant points are collected for the analysis during the total testing time of 100 min. For each data point, the frequency shift from the center frequency is calculated and the results were found to lie in a certain frequency range. The overall frequency range was divided into 40 bins of 10 kHz each. Based on the count of each frequency shift in a particular bin, we are able to get the event probability as shown in Fig. S3b. A nonlinear data fitting method with a Gaussian function is adopted to get a fitting curve. Through this method, the probability of a given frequency measurement lying in the range of $\pm$ 130 kHz (260 kHz in total) is calculated to be 90%.

Assuming that the immobilized and hybridized DNA double helix chains are all standing vertically on the gold delay area (illustrated in Fig. 1d), the occupied area $A_{DNA} = \pi R^2$ for a single DNA double helix structure can be obtained. A further assumption can be made that the DNA double helix structure behave as cylinders with an average radius of 1.0 nm and the gold surface of the delay area is all filled with vertical DNA molecule chains. In this way, the mass noise for a single DNA molecule is obtained from the equation $\Delta m_2 = \Delta m_2' \cdot A_{DNA}$. The average mass of a single base m_s is calculated from the equation $m_s = (M_{AT} + M_{CG})/(4 \cdot N_A)$, where the mass of hybridized base pair A,T and hybridized base pair C,G are respectively $M_{AT} = 669.44$ Da, $M_{CG} = 680.43$ Da, and N_A is the Avogadro constant.

The equivalent number of DNA base n for the mass noise Δm_2 can be obtained from $n = \Delta m_2 / m_s = 0.01$. This implies that the biosensor has a mass definition of 0.01 DNA bases or ~3 Da, i.e., the equivalent mass of 3 hydrogen atoms. The achieved atomic

resolution allows us to accurately monitor the adsorption of atoms without interference of systematic noise error brought by the biosensor itself. This is far beyond the requirement of single base or single molecule detection.

The proposed SAW biosensor is the first effort which utilizes such a high frequency of about 6.4 GHz, and this brings about two advantages. On one hand, the sensitivity is greatly improved as compared to low frequency devices such as quartz crystal microbalance (QCM) (Hepel, 1999). A higher frequency biosensor will cause a larger frequency shift for a certain mass, therefore the sensitivity is enhanced. Also, according to Eq. (2), the simultaneously increased noise floor, which is 260 kHz for the SAW biosensor, does not even have a comparable value to the frequency shift of single cell (about 500 kHz). Thus the increased noise floor will not have significant influence on the sensing ability in the detectable range. On the other hand, a higher frequency of the biosensor is partially obtained from the reduction of the device, and the overall dimension of the SAW device is significantly decreased compared to previous reported works. Moreover, the DNA detection shows that the SAW biosensor is capable of selective detection by immobilizing probe substances, such as DNA, protein, enzyme or immunity substance. The detection of cells is an evaluation of the biosensor's frequency response to ultralight mass. The repeated experiment shows the ability to recycle the device after multiple biological treatments and measurements. Both the experimental and analytical results have demonstrated that the SAW biosensor has the advantages of high sensitivity, high selectivity, repeatability and robustness.

4. Conclusions

A novel SAW biosensor operating at high-order mode has been proposed for atomic resolution and highly selective biomedical detection for the first time. The experimental results show a wide detectable concentration range and ultra-high detection sensitivity of 6.7×10^{-16} g/cm^2/Hz. With the achieved sensitivity, it is possible to sense a single DNA base. The detection of EMT6 cells and 3T3 cells is also studied to verify this ability. Therefore, multiple highly selective and highly sensitive detections will be achieved employing the mechanisms of probe and target DNA hybridization, protein and enzyme reaction, antigen and antibody specific binding, etc. (El-Ali et al., 2006; Gronewold et al., 2006; Park et al., 2008; Stern et al., 2010; Weart et al., 2007). Moreover, the simple fabrication process, small device feature-size and low requirement of samples for testing present our SAW devices as a promising alternative with strong versatility for future portable applications. Because the substrate property is sensitive to temperature, and the frequency shift with temperature variation is a main limitation of SAW biosensors, this influence is necessary to be studied. Temperature compensation should be introduced to overcome this shortcoming. In order to confirm the atomic resolution in experiment, the frequency response to a single atom is also an aspect of future work.

Acknowledgments

This work was supported by National Natural Science Foundation of China (61434001), 973 Program (2015CB352100), National Key Project of Science and Technology (2011ZX02403-002) and Special Fund for Agroscientic Research in the Public Interest (201303107) of China. M.A.M is additionally supported by the postdoctoral fellowship (PDF) program of the Natural Sciences and Engineering Research Council of Canada (NSERC).

Appendix A. Supplementary material

Supplementary data associated with this article can be found in the online version at http://dx.doi.org/10.1016/j.bios.2015.04.043

References

Aebersold, Ruedi, et al., 2003. Nature 422 (6928), 198–207.
Alivisatos, Paul, 2004. Nat. Biotechnol. 22 (1), 47–52.
Anker, Jeffrey N., et al., 2008. Nat. Mater. 7 (6), 442–453.
Campanella, Humberto, et al., 2006. Appl. Phys. Lett. 89 (3), 033507.
Chen, Kuan-I., et al., 2011. Nano Today 6 (2), 131–154.
de la Rica, Roberto, et al., 2009. Anal. Chem. 81 (24), 10167–10171.
Dong, Xiaochen, et al., 2010. Adv. Mater. 22 (14), 1649–1653.
Dow, Ali B. Alamin, et al., 2012. IEEE Trans. Nanotechnol. 11 (5), 979–984.
El-Ali, Jamil, et al., 2006. Nature 442 (7101), 403–411.
Feng, X.L., et al., 2008. Nat. Nanotechnol. 3 (6), 342–346.
Ferreira, Guilherme N.M., et al., 2009. Trends Biotechnol. 27 (12), 689–697.
Giljohann, et al., 2009. Nature 462 (7272), 461–464.
Gronewold, Thomas M.A., et al., 2006. Anal. Chem. 78 (14), 4865–4871.
Heller, Daniel A., et al., 2009. Nat. Nanotechnol. 4 (2), 114–120.
Hepel, M., 1999. Electrode-solution interface studied with electrochemical quartz crystal nanobalance In: Wieckowski, A. (Ed.), Interfacial Electrochemistry. Theory, Experiment and Applications. Marcel Dekker Inc., New York, pp. 599–630.
Jensen, K., et al., 2008. Nat. Nanotechnol. 3 (9), 533–537.
Kim, Sang-Gyu, et al., 2013. Biosens. Bioelectron. 50, 362–367.
Krishnamoorthy, et al., 2008. Biosens. Bioelectron. 24 (2), 313–318.
Lee, Hakho, et al., 2008. Nat. Med. 14 (8), 869–874.
Li, Mo, et al., 2007. Nat. Nanotechnol. 2 (2), 114–120.
Lu, Yuerui, et al., 2011. Nat. Commun. 2, 578.
Lucarelli, Fausto, et al., 2008. Anal. Chim. Acta 609 (2), 139–159.
Mannoor, Manu S., et al., 2012. Nat. Commun. 3, 763.
Muhammad, Mustafa, et al., 2011. J. Vac. Sci. Technol. B 29 (6), 06F304.
Naik, A.K., et al., 2009. Nat. Nanotechnol. 4 (7), 445–450.
Palankar, Raghavendra, et al., 2013. ACS Nano 7 (5), 4617–4628.
Park, Kidong, et al., 2008. Lab Chip 8 (7), 1034–1041.
Peng, Gang, et al., 2009. Nat. Nanotechnol. 4 (10), 669–673.
Peters, Robert, et al., 2013. J. Vac. Sci. Technol. B 31 (6), 06F407.
Peterson, Alexander W., et al., 2001. Nucleic Acids Res. 29 (24), 5163–5168.
Petrie, Jonathan R., et al., 2011. Appl. Phys. Lett. 99 (4), 043504.
Petrovykh, Dmitri Y., et al., 2003. J. Am. Chem. Soc. 125 (17), 5219–5226.
Rosi, Nathaniel L., et al., 2005. Chem. Rev. 105 (4), 1547–1562.
Shi, Ping, et al., 2010. Small 6 (22), 2598–2603.
Smith, Emily A., et al., 2001. Langmuir 17 (8), 2502–2507.
Stern, Eric, et al., 2010. Nat. Nanotechnol. 5 (2), 138–142.
Sun, Lijun, et al., 2013. Science 339 (6121), 786–791.
Venkatesan, Bala Murali, et al., 2011. Nat. Nanotechnol. 6 (10), 615–624.
Weart, Richard B., et al., 2007. Cell 130 (2), 335–347.
Yang, Y.T., et al., 2006. Nano Lett. 6 (4), 583–586.